Effect of filtered feedback on birhythmicity: Suppression of birhythmic oscillation

Debabrata Biswas,[1,*] Tanmoy Banerjee,[2,†] and Jürgen Kurths[3,4,‡]

[1]*Department of Physics, Rampurhat College, Birbhum 731224, West Bengal, India*

[2]*Chaos and Complex Systems Research Laboratory, Department of Physics, University of Burdwan, Burdwan 713 104, West Bengal, India*

[3]*Potsdam Institute for Climate Impact Research, Telegraphenberg, D-14415 Potsdam, Germany*

[4]*Institute of Physics, Humboldt University Berlin, D-12489 Berlin, Germany*

(Received 12 April 2019; published 14 June 2019)

The birhythmic oscillation, generally known as birhythmicity, arises in a plethora of physical, chemical, and biological systems. In this paper we investigate the effect of filtered feedback on birhythmicity as both are relevant in many living and engineering systems. We show that the presence of a low-pass filter in the feedback path of a birhythmic system suppresses birhythmicity and supports monorhythmic oscillations depending on the filtering parameter. Using harmonic decomposition and energy balance methods we determine the conditions for which birhythmicity is removed. We carry out a detailed bifurcation analysis to unveil the mechanism behind the quenching of birhythmic oscillations. Finally, we demonstrate our theoretical findings in analog simulation with electronic circuit. This study may have practical applications in quenching birhythmicity in several biochemical and physical systems.

DOI: 10.1103/PhysRevE.99.062210

I. INTRODUCTION

Birhythmicity is an interesting manifestation of multistability that arises in many natural and human-made systems [1–4]. According to the notion introduced by Prigogine [5], of four fundamental types of "dissipative structures" that occur in dynamical systems, multistability and particularly its complex oscillatory form, birhythmicity, special attention due to their ubiquity in physical and biological systems (the other three "structures" being temporal dissipative structure, spatial dissipative structure, and spatiotemporal structure; see the recent review by Goldbeter [6]). Therefore, understanding birhythmic oscillation has been an active topic of research in physics [7,8], chemistry [9], and biology [1,2]. The signature of birhythmicity is the coexistence of two stable limit cycles with different amplitudes and frequencies separated by an unstable limit cycle. Birhythmicity plays a significant role in living systems in maintaining different modes of oscillations to organize various biochemical processes in a varying environment [10]. A few examples of birhythmic oscillations that appear in living systems include the glycolytic oscillations and enzymatic reactions [1,2,9,11], intracellular Ca^{2+} oscillations [12], oscillations in the p53-Mdm2 network [13,14], the circadian oscillation in Period (PER) and Timeless (TIM) proteins in *Drosophila* [15], the cyclic AMP signaling system of the slime mold *Dictyostelium discoideum* [16], oscillatory generation of cyclic adenosine monophosphate (cAMP) [17], and rhythm arises in population dynamics [18]. Apart from living systems, many artificial systems (e.g., the wind-induced mechanical energy harvesting system [7,19]) exhibit birhythmic oscillations.

On the other hand, another important process that plays a crucial role in living and engineering systems is filtering, which typically arises in the feedback path—the feedback can be either self or mutual. In the context of oscillatory or rhythmic processes, the filtered-feedback is of much practical importance because a signal in its feedback path may suffer attenuation and dispersion, which result in a change of amplitude and (or) phase of the signal. If the signal suffers both attenuation and dispersion, then the coupling path can be modeled as a low-pass filter (LPF). Recent studies reveal that the feedback path governed by low-pass filter is inherently present in living systems, e.g., LPFs are a basic component of the musculoskeletal system of human body [20] and the abdominal ganglion of the crayfish contains LPFs in local feedback path [21]. On the other hand, in several engineering systems filtered-feedback plays a crucial role. For example, in phase-locked loops [22] low-pass filter in the feedback path is an essential building block, which eliminates noise and high-frequency signals. In laser systems filtered-feedback is widely used to achieve a stable single-frequency operating condition [23,24].

Although both birhythmicity and filtering (in feedback path) are relevant in dynamical systems, surprisingly, their interplay has not been studied much yet, whereas the effect of filtering in the context of other dynamical phenomena, e.g., synchronization [25–27], oscillation suppression and revival [28,29], and symmetry-breaking [30,31], has been explored in detail and the studies revealed that filtering leads to several interesting dynamical behaviors.

In this paper, we study the effect of low-pass filtering in the feedback path on the occurrence of birhythmic oscillations. We consider a paradigmatic model of birhythmic van der Pol oscillator, which has been widely employed in the studies

*debbisrs@gmail.com

†tbanerjee@phys.buruniv.ac.in

‡juergen.kurths@pik-potsdam.de

 ©2019 American Physical Society

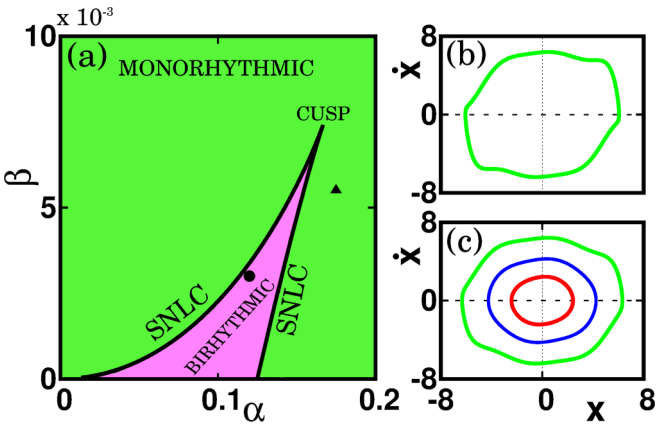

FIG. 1. (a) Two-parameter bifurcation diagram in α-β space for $\mu = 0.1$. Solid line represents saddle-node bifurcation of limit cycles and they meet at a codimension-2 cusp bifurcation point. (b) Monorhythmic oscillation for $\alpha = 0.175$ and $\beta = 0.0055$ [filled triangle in (a)]. (c) Birhythmic oscillation for $\alpha = 0.12$ and $\beta = 0.003$ [filled circle in (a)].

of birhythmicity [32–34], and show that the presence of a low-pass filter in the feedback path is detrimental for birhythmicity and conducive for monorhythmicity. We explore that the system changes from a birhythmic to a monorhythmic regime with a decreasing cut-off frequency of the LPF in a broad range of system parameters. We theoretically analyze the system using harmonic decomposition and energy balance methods and determine the critical value of the cut-off frequency of the low-pass filter that eliminates birhythmicity. We support our analysis by a numerical bifurcation analysis using the continuation package XPPAUT [35]. Finally, through an electronic circuit-based analog simulation, we demonstrate that our results holds well even in practical conditions where parameter fluctuation and noise are inevitable.

II. THE BIRHYTHMIC VAN DER POL OSCILLATOR

The birhythmic van der Pol (vdP) oscillator is given by the following equation [32,33,36]:

$$\ddot{x} - \mu f(x)\dot{x} + x = 0, \tag{1}$$

where $f(x) = 1 - x^2 + \alpha x^4 - \beta x^6$ is a nonlinear function and $\mu > 0$, $\alpha > 0$, $\beta > 0$ are parameters that determine the nonlinear damping.

The harmonic decomposition method considering $x(t) = A\cos\omega t$ leads to the following amplitude equation [37]:

$$\frac{5\beta}{64}A^6 - \frac{\alpha}{8}A^4 + \frac{1}{4}A^2 - 1 = 0, \tag{2}$$

which is independent of the parameter μ and represents the generic form of the codimension-2 bifurcation. The cusp type of codimension-2 bifurcation in the α-β parameter space is shown in Fig. 1(a). Birhythmicity emerges from the saddle-node bifurcation of the limit cycle (SNLC) (the solid black line in the figure). In the monorhythmic zone there exists only one limit cycle in the whole phase space [see Fig. 1(b)]. However, in the birhythmic zone there exist three limit cycles (LCs) of which two are stable and one is unstable. Among the two stable LCs, one has a smaller amplitude and the other has a larger one. The unstable LC lies between these two stable LCs and acts as the separatrix between them [see Fig. 1(c)].

III. EFFECT OF FILTERED-FEEDBACK ON BIRHYTHMICITY: MODEL AND ANALYSIS

We apply a low-pass filtering in the birhythmic van der Pol oscillator and the mathematical model reads

$$\ddot{x} - \mu f(x)\dot{x} + x + dz = 0, \tag{3a}$$

$$\dot{z} = \gamma(-z + x). \tag{3b}$$

In the above set of equations the system variable $x(t)$ of the birhythmic van der Pol oscillator is subjected to a LPF represented by Eq. (3b). The output $z(t)$ of the LPF is then fed back into the original system (3a) with the self-feedback strength d. Note that $d = 0$ indicates the absence of filtering in the birhythmic system; therefore, Eqs. (3) reduces to the original system given by (1). Equation (3b) represents the differential equation of a first-order LPF whose cut-off frequency is γ. If the input signal $x(t)$ has an angular frequency ω (say), then the output signal $z(t)$ will be phase shifted by $\varphi = \tan^{-1}(\omega/\gamma)$ and the gain of the filter (i.e., the absolute value of the ratio of output to input) will be $G = \frac{1}{\sqrt{1+\omega^2\gamma^{-2}}}$ [38]. In the limiting case for $\gamma \to \infty$, $G \to 1$, $z(t) = x(t)$, i.e, there is no filtering effect. On the other hand, $\gamma \to 0$ (or very small) means that the filter completely attenuates all the oscillatory components of the signal (i.e., filtering effect is stronger).

To understand the effect of γ on the dynamics of the system we apply the harmonic decomposition method [39]. For this let us assume the approximate solution of Eq. (3) as

$$x(t) = A\cos\omega t, \tag{4}$$

where ω is the natural frequency of the oscillator. As discussed earlier, the output of the low-pass filter $z(t)$ differs from $x(t)$ by amplitude and phase. However, for $\gamma > \omega$ the amplitude of the filtered signal, $z(t)$, remains almost the same as that of the original signal $x(t)$. Therefore, under this limit the LPF output has the same amplitude (A) but different phase (φ) and can be written as

$$z(t) = A\cos(\omega t + \varphi). \tag{5}$$

Substitution of Eqs. (4) and (5) into Eq. (3) yields

$$\begin{aligned}\left(1 + d - \omega^2 + \frac{d\omega^2}{\gamma\sqrt{\gamma^2+\omega^2}}\right)A\cos\omega t &= -\mu\omega\left(1 - \frac{1}{4}A^2 + \frac{\alpha}{8}A^4 - \frac{5\beta}{64}A^6\right)A\sin\omega t \\ &\quad - \frac{d\omega}{\sqrt{(\gamma^2+\omega^2)}}A\sin\omega t \\ &\quad + \mu\omega\left(\frac{1}{4}A^2 - \frac{3\alpha}{16}A^4 + \frac{9\beta}{64}A^6\right)A\sin 3\omega t \\ &\quad - \mu\omega\left(\frac{\alpha}{16}A^4 - \frac{5\beta}{64}A^6\right)A\sin 5\omega t \\ &\quad + \mu\omega\frac{\beta A^6}{64}A\sin 7\omega t. \end{aligned} \tag{6}$$

The higher harmonics may be considered as forcing terms, which diminish with increasing harmonics. Thus they can be ignored [39] and the above equation becomes

$$\left(1+d-\omega^2+\frac{d\omega^2}{\gamma\sqrt{\gamma^2+\omega^2}}\right)A\cos\omega t = -\mu\omega\left(1-\frac{1}{4}A^2+\frac{\alpha}{8}A^4-\frac{5\beta}{64}A^6\right)A\sin\omega t - \frac{d\omega}{\sqrt{(\gamma^2+\omega^2)}}A\sin\omega t+\mathcal{H}, \quad (7)$$

where $\mathcal{H}$ denotes the higher harmonic terms. Equation (7) refers to the following frequency and amplitude equations, respectively:

$$1+d-\omega^2+\frac{d\omega^2}{\gamma\sqrt{\gamma^2+\omega^2}}=0 \quad (8)$$

and

$$\mu\left(1-\frac{1}{4}A^2+\frac{\alpha}{8}A^4-\frac{5\beta}{64}A^6\right)+\frac{d}{\sqrt{(\gamma^2+\omega^2)}}=0. \quad (9)$$

From (8) note that for $d=0$, i.e., no filter is employed in the system, $\omega^2=1$, which gives the normal birhythmic vdP oscillator of unit eigenfrequency given by Eq. (1). Also, for larger values of γ, Eq. (9) gives $\omega^2=(d+1)$: This is physically justified as in this limit $z(t)=x(t)$, and Eq. (3) now has an effective eigenfrequency $\omega=\sqrt{d+1}$. Also, from (9) it can be seen that in the weak filtering case, i.e., large-γ limit, the amplitude equation reduces to (2).

The frequency in the harmonic limit reduces to $\omega=1$. The three limit cycles (two stable, one unstable) are results of the three roots of the amplitude equation. To get an idea of the amplitude of the limit cycles, we analyze the stability of the system using the energy balance method [40]. In order to analyze the system, we rewrite Eq. (3) as the following equation:

$$\ddot{x}-\mu f(x)\dot{x}+x+d\left(x-\frac{\dot{z}}{\gamma}\right)=0. \quad (10)$$

The solution of Eq. (10) for $\mu=0$ and $d=0$ is given by

$$x(t)=A\cos(t+\phi) \quad (11)$$

and

$$z(t)\equiv\text{LPF output of } x(t)=A\cos(t+\psi), \quad (12)$$

where ϕ is the initial phase and $\psi=\phi+\varphi$ is the phase of the LPF output. For convenience we may consider $\phi=0$, hence $\psi=\varphi$.

The change in energy ΔE in one period $0\leqslant t\leqslant T(=2\pi)$ is found by considering the term $[\mu f(x)-d(x-\dot{z}/\gamma)]$ as the external forcing term. Thus the change in energy is given as

$$\Delta E = E(T)-E(0), = \int_0^T[\mu f(x)-d(x-\dot{z}/\gamma)]\dot{x}dt. \quad (13)$$

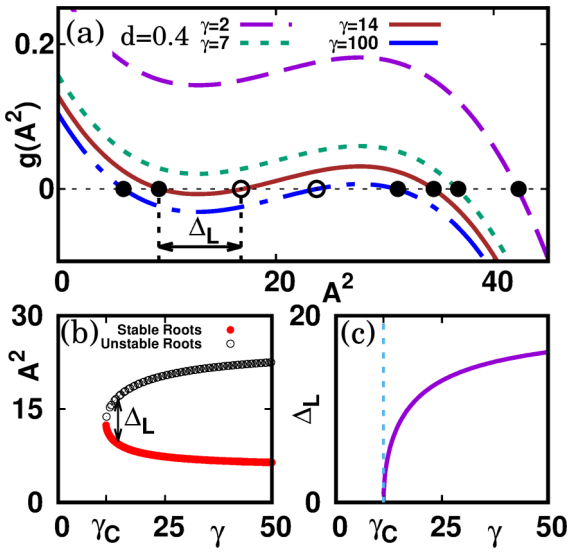

FIG. 2. (a) Plot of $f(A^2)$-A^2 for the parameter set $\mu=0.1$, $\alpha=0.114$, $\beta=0.003$, and $d=0.4$ for different values of the cut-off frequency, γ. Solid (hollow) circle indicates stable (unstable) solutions. Δ_L denotes the distance between the left-most stable root and the unstable root. (b) Plot of the left-most stable and unstable roots in the γ-A^2 plane. (c) Variation of Δ_L with γ: At $\gamma=\gamma_c$ (here $\gamma_c=11.09$), Δ_L becomes zero and saddle node bifurcation of limit cycles occur.

For a periodic solution (limit cycle) one gets $\Delta E=0$. Thus Eq. (13) on substitution of Eqs. (11) and (12) yields

$$f(A^2)\equiv\mu\left(1-\frac{1}{4}A^2+\frac{\alpha}{8}A^4-\frac{5\beta}{64}A^6\right)+\frac{d}{\sqrt{(\gamma^2+1)}}=0. \quad (14)$$

It is worth noting that Eq. (14) and Eq. (9) are equivalent for $\omega=1$.

The presence of limit cycles and their stability can be determined by solving Eq. (14). To solve it we use graphical method by plotting $f(A^2)$ vs. A^2 as shown in Fig. 2 (for $\mu=0.1$, $\alpha=0.114$, $\beta=0.003$, and $d=0.4$). The zero-crossing points of the curves determine the number of limit cycles: The number of zero crossing is the number of limit cycles, whereas the stability of the limit cycles is determined by their slope at the zero crossing points: A negative slope means that the limit cycle is stable and a positive slope denotes an unstable limit cycle. In Fig. 2(a) we show how birhythmic behavior changes into monorhythmic one under stronger filtering effect (i.e., decreasing γ). The lower curve [long-short dashed line (blue)] is for $\gamma=100$, i.e., a much higher value of cut-off frequency (in comparison with $\omega=1$, i.e., the intrinsic frequency of the oscillator). The curve shows three zero-crossing points: The points denoted by solid circles indicate the solutions for stable limit cycles due to the negative slope at those points and that in the middle denoted by a hollow circle indicates the unstable limit cycle. As we make the filtering effect stronger by decreasing γ the curve moves upward. See the solid line for $\gamma=14$: Although it still shows birhytmicity (i.e., two stable and one unstable limit cycles), the left-most root (denoted by the solid circle) comes closer the middle root

(denoted by the hollow circle). Let us denote the distance (in the A^2 axis) between these two roots as Δ_L [see Fig. 2(a)]. Figure 2(b) demonstrates the variation in the position of the two left-most roots in the A^2 axis with γ: As γ approaches γ_c (say) from a higher value the roots come closer, i.e., Δ_L decreases, and at $\gamma = \gamma_c$ they collide making $\Delta_L = 0$. Figure 2(c) shows the variation of Δ_L with γ. Hence, at $\gamma = \gamma_c$ a SNLC occurs where the inner stable limit cycle is destroyed by collision with the unstable limit cycle [note that one can derive the expression of γ_c by minimizing $f(A^2)$ from Eq. 14]. Therefore, for $\gamma \leqslant \gamma_c$, the stable limit cycle (indicated by the rightmost root–solid circle) is the only oscillation present in the system, and thus the system is in the monorhythmic zone. Two exemplary curves for $\gamma = 7$ (short dash) and $\gamma = 2$ (long dash) are shown in Fig. 2(a) showing monorhythmic oscillations. Hence a stronger low-pass filtering (i.e., a smaller γ) actually suppresses birhythmic oscillations.

IV. NUMERICAL BIFURCATION ANALYSIS

In this section we investigate the effect of low-pass filter parameter γ on the birhythmic dynamics by exploring bifurcation scenarios of the birhythmic van der Pol system [Eq. (3)] using continuation package XPPAUT. At first we explore the dynamics in the d-γ space for fixed nonlinear system parameters (i.e., μ, α, and β). Next, we investigate the detailed bifurcation scenarios which arise due to the variation of γ and the nonlinear system parameters for a fixed feedback strength d.

A. Dynamics in d-γ space

To study the bifurcation scenario, in the d-γ space, we keep the original system in its birhythmic zone by fixing $\mu = 0.1$, $\alpha = 0.114$, and $\beta = 0.003$ (cf. Fig. 1). The bifurcation scenarios are shown in Figs. 3(a) and 3(b). The two parameter bifurcation diagram of Fig. 3(a) demonstrates that the SNLC curve (shown in solid black line) subdivides the whole parameter space into two regimes, namely a birhythmic zone and a monorhythmic zone.

It can be seen from Fig. 3(a) that for $\gamma \to \infty$, i.e., in the absence of filtering, the system is always in the birhythmic zone. However, as we decrease the cut-off frequency γ (i.e., making the filtering effect stronger), the monorhythmic zone becomes wider thus suppressing the birhythmic regime. Note that at $\gamma = 1$ and $d = d_c$ we have the maximum zone of monorhythmicity. It is also interesting to note that for $\gamma < 1$ a smaller zone of birhythmicity reappears even for $d > d_c$: This is because here we consider $\omega = 1$, therefore, for $\gamma < \omega(= 1)$ the low-pass filter greatly attenuates the system's oscillation and makes $z(t)$ much smaller. However, in that case a comparatively larger d ensures monorhythmicity.

To get a more clearer view of the bifurcation scenario, we draw the one-parameter bifurcation diagram in Fig. 3(b) with γ for an exemplary value $d = 0.4$ [along the broken vertical line of Fig. 3(a)]. The system is birhythmic for $\gamma > \gamma_c$: Here $\gamma_c = 11.09$, which is in agreement with the analytical result of Sec. III [see Fig. 2(c)]. In this zone two stable limit cycles [shown in light gray (green) line] are separated by

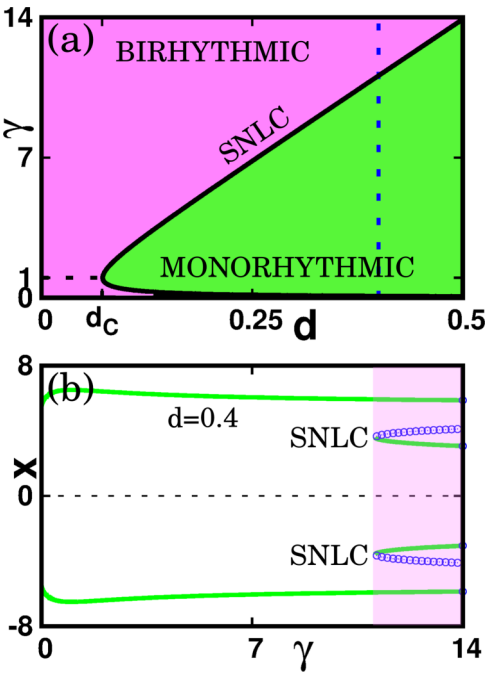

FIG. 3. (a) Two parameter bifurcation diagram in d-γ space for $\mu = 0.1$, $\alpha = 0.114$, and $\beta = 0.003$. For $\gamma = 1$ and $d = d_c$ monorhythmic zone has maximum spreading. (b) One-parameter bifurcation diagram with γ for $d = 0.4$ [along the vertical broken line in Fig. 3(a)]; at $\gamma = \gamma_c = 11.09$ SNLC occurs [in agreement with the analytical result of Fig. 2(c)].

an unstable limit cycle [shown in dark gray (blue) line]. At $\gamma = \gamma_c$ the inner stable limit cycle collides with the unstable limit cycle and they destroy each other. Therefore, for $\gamma < \gamma_c$ only monorhythmic oscillation exists. Hence, with the proper choice of the cut-off frequency of the filter, γ, the birhythmicity is suppressed and a complete monorhythmic oscillation prevails.

Two representative time series for two exemplary values of the cut-off frequency γ are shown in Figs. 4(a) and 4(b) and Figs. 4(c) and 4(d) at $d = 0.4$ ($\mu = 0.1$, $\alpha = 0.114$, $\beta = 0.003$). Figures 4(a) and 4(b) are for $\gamma = 14$: The time series is shown in Fig. 4(a) and the corresponding phase plane plot in x-$\dot{x}$ space is shown in Fig. 4(b). The figure shows the results of two initial conditions (ICs), namely one around the origin, $\mathcal{I}_S \equiv (x_0, \dot{x}_0) = (0.1, 0)$ (to target the small-amplitude LC) and another far from the origin, $\mathcal{I}_L \equiv (x_0, \dot{x}_0) = (7, 0)$ (to target the large-amplitude LC). In Figs. 4 the dark gray (red) line shows the small-amplitude oscillation corresponding to the IC $\mathcal{I}_S$ and the lighter gray (green) line shows the large-amplitude oscillation for the IC $\mathcal{I}_L$. The time series and phase plane plots clearly depict the presence of birhythmicity in the system. The solid (blue) line in Fig. 4(b) in between two stable LCs separating the large-amplitude oscillation from the small-amplitude one indicates the unstable LC.

Figures 4(c) and 4(d) are for $\gamma = 2$: Here we see that at the lower value of γ (i.e., for stronger filtering) the system loses its birhythmic nature and monorhythmicity comes into play. The time series [Fig. 4(c)] and phase plane plot [Fig. 4(d)] clearly depict the occurrence of monorhythmicity: For any initial condition the system ends up into a single limit cycle.

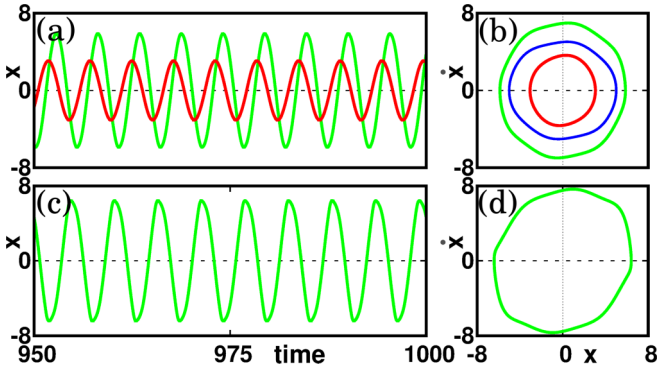

FIG. 4. Time series and phase plane plots. [(a) and (b)] $\gamma = 14$: Birhythmic oscillations, the trajectory in the middle of two LCs in (b) represents unstable LC. [(c) and (d)] $\gamma = 2$: A single monorhythmic LC. The dark gray (red) line is for the initial conditions $\mathcal{I}_S \equiv (x_0, \dot{x}_0) = (0.1, 0)$; the light gray (green) line is for the initial condition $\mathcal{I}_L \equiv (x_0, \dot{x}_0) = (7, 0)$. Note that in (d) both initial conditions result in a single LC confirming a monorhythmic oscillation. Other parameters are $\mu = 0.1$, $\alpha = 0.114$, $\beta = 0.003$, and $d = 0.4$.

B. Interplay of filtering (γ) and the nonlinear damping parameters

Next, we explore the effect of filtering parameter on the birhythmic behavior over a range of nonlinear damping parameters (e.g., μ, α, and β). For this we keep the filtering strength d fixed at $d = 0.4$ and study the bifurcation scenarios in the μ-γ, α-γ, and β-γ space. Figure 5(a) gives the two-parameter bifurcation in the μ-γ space (for $\alpha = 0.114$ and $\beta = 0.003$): It shows that with decreasing γ the SNLC curve that separates the monorhythmic zone from the birhythmic one moves toward right thus suppressing the area of birhythmicity. Figure 5(b) depicts the dynamics in the α-γ space (for $\mu = 0.1$ and $\beta = 0.003$) and Fig. 5(c) shows the same

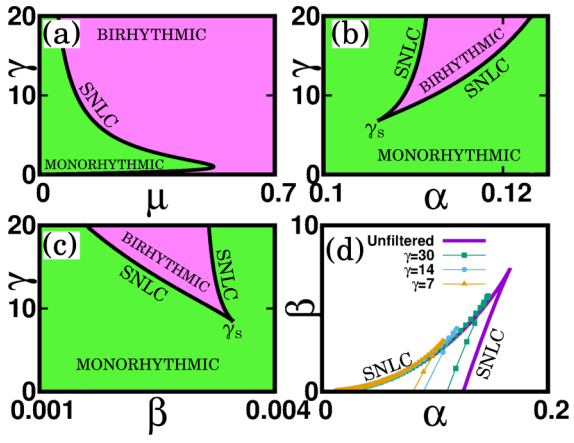

FIG. 5. (a) Two-parameter bifurcation diagram in μ-γ space for $\alpha = 0.114$, $\beta = 0.003$, and $d = 0.4$; (b) two-parameter bifurcation diagram in α-γ space (for $\mu = 0.1$, $\beta = 0.003$, and $d = 0.4$). (c) Two-parameter bifurcation diagram in β-γ space (for $\mu = 0.1$, $\alpha = 0.114$, and $d = 0.4$). (d) Two-parameter bifurcation diagram in α-β space with (solid line) and without filtering ($\mu = 0.1$ and $d = 0.4$): A decreasing γ suppresses the birhythmic zone.

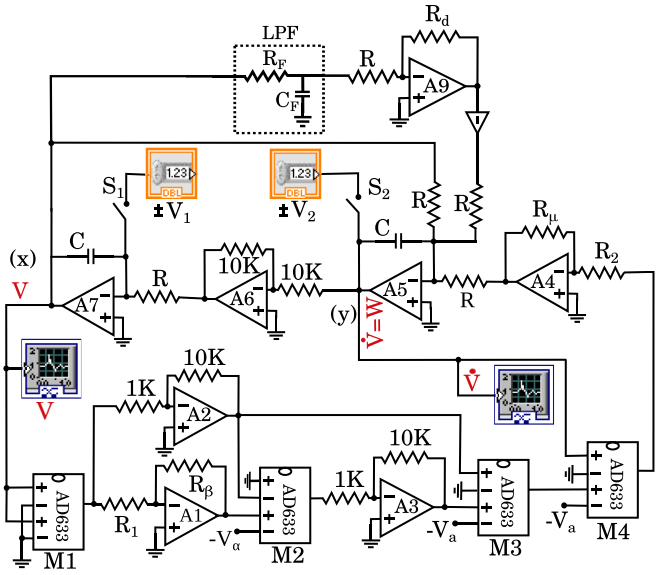

FIG. 6. The experimental circuit diagram. It is made compatible to be controlled and acquired by DAQ and Labview. For description and parameter values see text.

in the β-γ (for $\mu = 0.1$ and $\alpha = 0.114$). Interestingly, both graphs demonstrate that with decreasing γ the two SNLC curves approach each other and meet at a point γ_S through a *codimension-2* cusp bifurcation and therefore destroy birhythmicity.

Finally, in Fig. 5(d) we demonstrate the effect of cut-off frequency γ on the birhythmic dynamics in the α-β parameter space. The solid line represents the SNLC curve for the original (unfiltered) system which is the same as Fig. 1(a) (note that the birhythmic zone is below the SNLC curve). As we decrease γ the area contained by the SNLC curve becomes lesser making the birhythmic zone smaller. This is shown in Fig. 5(d) for three representative values of γ. For a much lesser γ ($<\gamma_c$) byrhythmic zone is completely destroyed (not shown in the figure). Therefore, we can infer that a proper choice of γ can eliminate the birhythmic oscillation in the system over a wider zone of nonlinear damping parameters.

V. ANALOG SIMULATION

The experimental observation of birhythmicity is very subtle due to the inherent noise and fluctuations in a real system [41]. Specially, in biological setup the timescale associated with birhythmic oscillations may vary from few minutes to 96 h [3] thus making it difficult to observe it in biological experiments. In this context, electronic circuit-based analog simulation provides a useful platform to demonstrate birhythmicity. In general, several important theoretical findings in nonlinear dynamics are tested in electronic circuit-based experiments as they generally demonstrate the robustness of the predicted results against parameter fluctuations, measurement and dynamical noise, and nonideal circuit behaviors [42–45]. Here also we demonstrate our theoretical results in electronic circuit-based analog simulation. Figure 6 shows the detailed circuit diagram implemented in a bread-board that emulates

Eqs. (3). We use AD633JN multiplier IC (M1-M4) and TL074 opamps (A1–A6).

Using Kirchhoff's voltage and current law, the following circuit equations are constructed:

$$RC\frac{dV}{dt} = W, \tag{15a}$$

$$RC\frac{dW}{dt} = \frac{R_\mu}{10R_2}\left(V_a - \frac{V_a}{10}V^2 + \frac{V_\alpha}{10}V^4 - \frac{R_\beta}{R_1}V^6\right)W - V - \frac{R_d}{R}S, \tag{15b}$$

$$RC\frac{dS}{dt} = \frac{CR}{C_F R_F}(-S + V). \tag{15c}$$

The above equation becomes dimensionless for the following substitutions: $t = \frac{t}{RC}$, $x = \frac{V}{V_{\rm sat}}$, $y = \frac{W}{V_{\rm sat}}$, $z = \frac{S}{V_{\rm sat}}$, $\frac{R_\mu}{10R_2} = \mu$, $\frac{R_d}{R} = d$, $V_a = a$, $\alpha = \frac{V_\alpha}{10}$, $\frac{R_\beta}{10R_1} = \beta$, and $\gamma = \frac{RC}{R_F C_F}$; with these substitutions and rescaling necessary for the experimentation, Eq. (15) is equivalent to Eq. (3).

The experiment is carried out in the following way. We implement the proposed birhythmic circuit in hardware and make arrangements to acquire the real-time data in a computer through a data acquisition (DAQ) system with LabView environment [46]. To control the initial conditions in the circuit, we use an arrangement of dual relay and control the on-off time of it by programming a microcontroller (Arduino Uno) [47]. The outputs from the relays are connected to the integrator (A5 and A7) terminals of the circuit. The capacitors C in the integrators are then charged to desired voltage levels (set through DAQ) by making both relays ON for a certain time. During this period the capacitors are charged to the required voltages, which serve as initial conditions to the circuit. In the normal mode of operation the relays are in the OFF condition. For the experiment we use the following values of the circuit components: $R_\mu = 296\ \Omega$, $R_\beta = 1.06\ \text{k}\Omega$, $R_1 = 1\ \text{k}\Omega$, $R_2 = 100\ \Omega$, $R = 10\ \text{k}\Omega$, $C = 0.1\ \mu\text{F}$, $V_\alpha = -1.247$ V, $V_a = -301.5$ mV, and $C_F = 0.2\ \mu\text{F}$. We fix the value of d by fixing $R_d = 203.5\ \Omega$.

The value of the LPF parameter γ is varied by varying the precession potentiometer R_F. In agreement with the theory (Secs. III and IV), we observe that for lower values of R_F (i.e., higher values of γ) the system is birhythmic in nature. We demonstrate the scenario for an exemplary value of $R_F = 18.25\ \text{k}\Omega$. To observe birhythmic oscillation, at first we feed the initial condition $\mathcal{I}_L \equiv (V_1, V_2) = (4.2V, 0.2V)$ in the circuit (using relays); in this condition the system undergoes oscillations with larger-amplitude LC. Next, to target the small-amplitude limit cycle the circuit is fed with the initial condition $\mathcal{I}_S \equiv (V_1, V_2) = (0.2V, 0.2V)$ and it indeed results in the inner small-amplitude LC. Figures 7(a) and 7(b), respectively, demonstrate the experimental time series and phase plane plots of birhythmic oscillations: The large LC appears for $\mathcal{I}_L$ and the smaller LC comes for $\mathcal{I}_S$. This results are in accordance with the numerical time series of Figs. 4(a) and 4(b).

Next, we decrease the value of γ by increasing the value of R_F: We set $R_F = 52.6\ \text{k}\Omega$ and keep all other parameters the same as before. We observe that for both initial conditions $\mathcal{I}_L$ and $\mathcal{I}_S$ the circuit exhibits only a single limit cycle [see Figs. 7(c) and 7(d)]. The scenarios are in accordance with the numerical time series of Figs. 4(c) and 4(d).

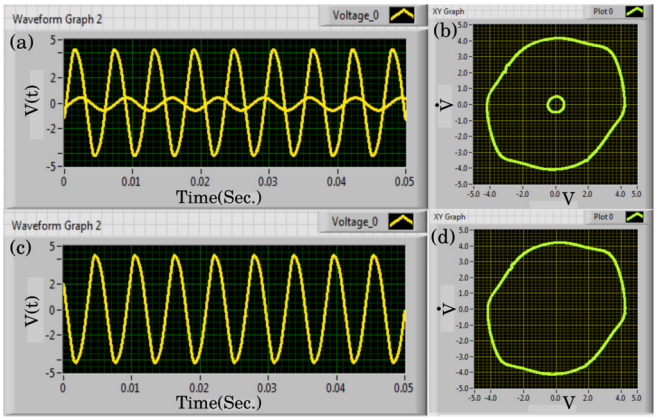

FIG. 7. The experimental time series and phase plane diagrams. [(a) and (b)] $R_F = 18.25\ \text{k}\Omega$: Birhythmic oscillations. [(c) and (d)] $R_F = 52.6\ \text{k}\Omega$: Monorhythmic oscillations with large-amplitude single LC. The initial conditions are $\mathcal{I}_L \equiv (V_1, V_2) = (4.2V, 0.2V)$ for large-amplitude LC and $\mathcal{I}_S \equiv (V_1, V_2) = (0.2V, 0.2V)$ for small-amplitude LC. For other parameters see text.

VI. CONCLUSION

In this paper we have studied the effect of low-pass filtering in the feedback path on the occurrence of birhythmicity. Using rigorous analytical techniques we have established that low-pass filtering in the feedback path is capable of suppressing birhythmic oscillations. A detailed numerical bifurcation analysis has been carried out to establish the mechanism behind the quenching of birhythmicity in the system. We have demonstrated our results in the electronic circuit-based analog simulation. Both theory and circuit experiment established that for some properly chosen cut-off frequency of the low-pass filter the birhythmicity can be suppressed completely.

We also verified (results not shown here) the effect of low-pass filtered-feedback in a practical system, namely the energy harvesting system [7], which is modeled by a modified version of birhythmic van der Pol oscillator, and got qualitatively the similar results. Our study also suggests that the low-pass filtering can be employed as an efficient control technique for birhythmicity (or other forms of multistability): By wishfully employing low-pass filter and tuning its cut-off frequency one can suppress birhythmicity where it limits the efficiency of a system and therefore is not desirable (e.g., in engineering systems [34,48]).

Our study can also be extended to other established models of birhythmicity, e.g., the glycolytic oscillators and enzymatic reactions model [1,2], and p53-Mdm2 network model [13,14]. However, before making any conclusive statement on the possible outcome, one needs to understand the feasibility and origin of filtering in those biological systems. Further, recently, bi- and trirhythmic oscillations have been reported in coupled circadian–cell cycle clocks [3]. We believe that, apart from birhythmicity, our study may have potential applications in controlling several other forms of *multirhythmic* oscillations in biochemical and physical systems.

[1] A. Goldbeter, *Biochemical Oscillations and Cellular Rythms: The Molecular Basis of Periodic and Chaotic Behavior* (Cambridge University Press, Cambridge, 1996).
[2] A. Goldbeter, Nature **420**, 238 (2002).
[3] J. Yan and A. Goldbeter, J. R. Soc. Interface **16**, 20180835 (2019).
[4] A. N. Pisarchik and U. Feudel, Phys. Rep. **540**, 167 (2014).
[5] I. Prigogine, in *Theoretical Physics and Biology*, edited by M. Marois (Wiley Interscience, New York, 1969).
[6] A. Goldbeter, Phil. Trans. R. Soc. A **376**, 20170376 (2018).
[7] C. A. K. Kwuimy and C. Nataraj, in *Structural Nonlinear Dynamics and Diagnosis*, edited by M. Belhaq (Springer International, Switzerland, 2015), Vol. 168, pp. 97–123.
[8] O. V. Pountougnigni, R. Yamapi, G. Filatrella, and C. Tchawoua, Phys. Rev. E **99**, 032220 (2019).
[9] S. Kar and D. S. Ray, Europhys. Lett. **67**, 137 (2004).
[10] M. Alamgir and I. Epstein, J. Am. Chem. Soc. **105**, 2500 (1983).
[11] S. Kar and D. S. Ray, Phys. Rev. Lett. **90**, 238102 (2003).
[12] A. N. Pisarchik, R. Jaimes-Reátegui, J. R. Villalobos-Salazar, J. H. García-López, and S. Boccaletti, Phys. Rev. Lett. **96**, 244102 (2006).
[13] W. Abou-Jaoudé, D. Ouattara, and M. Kaufman, J. Theor. Biol. **258**, 561 (2009).
[14] B. V. D. Lane and A. J. Levine, Nature **408**, 307 (2000).
[15] J. C. Leloup and A. Goldbeter, J. Theor. Biol. **198**, 445 (1999).
[16] A. Goldbeter and J. L. Martie, FEBS Lett. **191**, 149 (1985).
[17] J. L. Martiel and A. Goldbeter, Biophys. J. **52**, 807 (1987).
[18] R. Arumugam, T. Banerjee, and P. Dutta, Eur. Phys. J. Spec. Top. **226**, 2145 (2017).
[19] D. Biswas, T. Banerjee, and J. Kurths, Chaos **27**, 063110 (2017).
[20] A. M. Nakashima, M. J. Borland, and S. M. Abel, Ind. Health **45**, 318 (2007).
[21] L. Stark, *Neurological Control Systems: Studies in Bioengineering* (Plenum Press, New York, 1968).
[22] T. Banerjee, B. Paul, and B. C. Sarkar, Chaos **24**, 013116 (2014).
[23] H. Erzgraber and B. Krauskopf, Optics Lett. **32**, 2441 (2007).
[24] J. Zhao, D. Lenstra, R. Santos, M. J. Wale, M. K. Smit, and X. J. M. Leijtens, Opt. Expr. **20**, B270 (2012).
[25] M.-Y. Kim, C. Sramek, A. Uchida, and R. Roy, Phys. Rev. E **74**, 016211 (2006).
[26] M. C. Soriano, F. Ruiz-Oliveras, P. Colet, and C. R. Mirasso, Phys. Rev. E **78**, 046218 (2008).
[27] Y. Takiguchi, K. Ohyagi, and J. Ohtsubo, Optics Lett. **28**, 319 (2003).
[28] W. Zou, M. Zhan, and J. Kurths, Phys. Rev. E **95**, 062206 (2017).
[29] W. Zou, J. L. Ocampo-Espindola, D. V. Senthilkumar, I. Z. Kiss, M. Zhan, and J. Kurths, Phys. Rev. E **99**, 032214 (2019).
[30] T. Banerjee, D. Biswas, D. Ghosh, B. Bandyopadhyay, and J. Kurths, Phys. Rev. E **97**, 042218 (2018).
[31] T. Banerjee, B. Bandyopadhyay, A. Zakharova, and E. Schöll, Front. Appl. Math. Stat. **5**, 8 (2019).
[32] F. Kaiser and C. Eichwald, Int. J. Bifurcat. Chaos Appl. Sci. Eng. **01**, 485 (1991).
[33] C. Eichwald and F. Kaiser, Int. J. Bifurcat. Chaos Appl. Sci. Eng. **01**, 711 (1991).
[34] P. Ghosh, S. Sen, S. S. Riaz, and D. S. Ray, Phys. Rev. E **83**, 036205 (2011).
[35] B. Ermentrout, *Simulating, Analyzing, and Animating Dynamical Systems: A Guide to Xppaut for Researchers and Students (Software, Environments, Tools)* (SIAM Press, Philadelphia, PA, 2002).
[36] D. Biswas, T. Banerjee, and J. Kurths, Phys. Rev. E **94**, 042226 (2016).
[37] H. G. E. Kadji, J. B. C. Orou, R. Yamapi, and P. Woafo, Chaos Solitons Fractals **32**, 862 (2007).
[38] A. S. Sedra and K. C. Smith, *Microelectronic Circuits* (Oxford University Press, Oxford, UK, 2003).
[39] D. W. Jordan and P. Smith, *Nonlinear Ordinary Differential Equations* (Oxford University Press, New York, 1999).
[40] R. Yamapi, B. R. N. Nbendjo, and H. G. E. Kadji, Int. J. Bif. Chaos **17**, 1343 (2007).
[41] O. Decroly and A. Goldbeter, Proc. Natl. Acad. Sci. USA **79**, 6917 (1982).
[42] U. Parlitz, L. Junge, W. Lauterborn, and L. Kocarev, Phys. Rev. E **54**, 2115 (1996).
[43] D. V. Ramana Reddy, A. Sen, and G. L. Johnston, Phys. Rev. Lett. **85**, 3381 (2000).
[44] L. V. Gambuzza, A. Buscarino, S. Chessari, L. Fortuna, R. Meucci, and M. Frasca, Phys. Rev. E **90**, 032905 (2014).
[45] T. Stankovski, P. V. E. McClintock, and A. Stefanovska, Phys. Rev. E **89**, 062909 (2014).
[46] N. Instruments, *Labview: Data Acquisition Basics Manual* (National Instruments, Austin, 1996).
[47] M. Banzi, *Getting Started with Arduino*, 2nd ed. (Make Books, Sebastopol, CA, 2011).
[48] R. Sevilla-Escoboza, A. N. Pisarchik, R. Jaimes-Reátegui, and G. Huerta-Cuellar, Proc. R. Soc. Lond. A **471**, 20150005 (2015); A. N. Pisarchik and B. K. Goswami, Phys. Rev. Lett. **84**, 1423 (2000); A. N. Pisarchik, Phys. Rev. E **64**, 046203 (2001).